ISSN 2072-5981
doi: 10.26907/mrsej

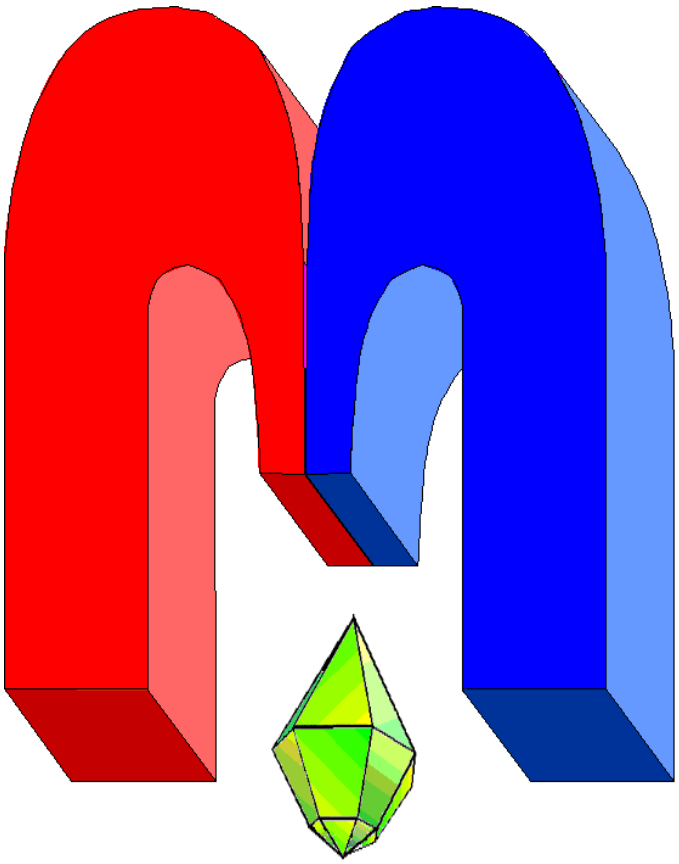

Magnetic Resonance in Solids

Electronic Journal

Volume ***28***
Issue ***1***
Article No ***26102***
1-10 pages
2026
doi: **10.26907/mrsej-26102**

http://mrsej.ru
http://mrsej.kpfu.ru

Established and published by Kazan University*
Endorsed by International Society of Magnetic Resonance (ISMAR)
Registered by Russian Federation Committee on Press (#015140), August 2, 1996
First Issue appeared on July 25, 1997

"***Magnetic Resonance in Solids. Electronic Journal***" (**MRS*ej***) is a peer-reviewed, all electronic journal, publishing articles which meet the highest standards of scientific quality in the field of basic research of a magnetic resonance in solids and related phenomena.

Indexed and abstracted by
Web of Science (*ESCI*, Clarivate Analytics, from 2015), *Scopus* (Elsevier, from 2012), *RusIndexSC* (*eLibrary*, from 2006), *Google Scholar*, *DOAJ*, *ROAD*, *CyberLeninka* (from 2006), *SCImago Journal & Country Rank*, etc.

---

* Address: "Magnetic Resonance in Solids. Electronic Journal", Kazan Federal University; Kremlevskaya str., 18; Kazan 420008, Russia

† In Kazan University the Electron Paramagnetic Resonance (EPR) was discovered by Zavoisky E.K. in 1944.

‡ This paper was selected at the International Conference "Modern Development of Magnetic Resonance 2025", September 29 -- October 3, 2025, Kazan, Russia.

Effect of hydrothermal treatment temperature on the structure and magnetic properties of LaF_3 nanoparticles†

A.M. Garaeva, B.M. Mukhamadullin, E.I. Boltenkova*, V.V. Kuzmin, F.F. Murzakhanov, G.V. Mamin, E.M. Alakshin

Kazan Federal University, Kazan 420008, Russian Federation

**E-mail: katarina.boltenkova@gmail.com*

(received April 22, 2026; revised April 30, 2026; accepted May 2, 2026; published May 3, 2026)

The effect of the hydrothermal treatment temperature of a colloidal solution of LaF_3 nanoparticles in an autoclave (60–140°C) on the particle size, the size of the coherent scattering region, and the concentration of paramagnetic centers has been studied. The samples were characterized using X-ray diffraction, transmission electron microscopy and magnetic resonance methods. The optimal hydrothermal treatment temperature has been determined to obtain particles with the largest size, best crystallinity, and minimum paramagnetic center content for practical applications. Theoretical estimates of the ^{19}F nuclear magnetic relaxation times for synthesized LaF_3 samples are presented, which are in good agreement with experimental data. The work may be useful in understanding the effect of hydrothermal treatment on the structure and magnetic interactions in nanoscale fluorides.

PACS: 61.46.+w, 75.75.-c

Keywords: nanoparticles, LaF_3, NMR, nuclear magnetic relaxation, rare-earth trifluorides, EPR, paramagnetic centers

1. Introduction

Lanthanum fluoride LaF_3 nanoparticles are a multifunctional material with a wide range of applications. The unique properties of LaF_3, such as the ability of its crystal lattice to substitute La^{3+} ions with other rare earth ions, make it valuable in materials engineering. LaF_3 nanoparticles doped with various impurities exhibit intense luminescence, which allows them to be used in optoelectronics (lasers, fiber amplifiers) [1]. LaF_3 can be used in biomedicine as a non-toxic fluorescent probe for cell imaging and theranostics, combining diagnostics and targeted drug delivery [2–4]. LaF_3 also serves as an ideal matrix for spectroscopic studies of the optical and magnetic properties of rare earth ions [5–10]. LaF_3 nanoparticles have low toxicity [11,12], high chemical and thermal stability [13], transparency over a wide spectral range [13, 14], and ease of doping with rare earth ions [5, 15, 16]. An important functional property of LaF_3 is its fast ionic transport: the material is a superionic conductor with a vacancy-mediated fluorine-ion migration mechanism, exhibiting purely anionic conductivity [17]. Thus, LaF_3 particles, due to the ability to fine-tune their properties through control of size, morphology, and doping, find application in a wide variety of fields, from medicine to electronics.

However, for the wide range of LaF_3 applications, it is necessary to synthesize particles that will have high crystallinity with a minimum number of defects. The presence of additional paramagnetic centers (transition metal impurities, uncontrolled rare earth ions, surface defects, OH groups or F-centers) can critically reduce the sample quality, negating the material advantages in key applications. For example, magnetic interactions (spin-spin and spin-lattice) between the paramagnetic center and the activator ion lead to fluctuations in the local crystal field. This causes inhomogeneous broadening of optical transitions, which is critical for laser media [18]. Paramagnetic impurities associated with defect act as effective energy acceptors, create additional channels of nonradiative relaxation, thereby reducing the quantum yield of

†This paper was selected at the International Conference "Modern Development of Magnetic Resonance 2025", September 29 – October 3, 2025, Kazan, Russia. The guest Editor, Prof. M.R. Gafurov, was responsible for the publication, which was reviewed according to the standard MRSej procedure.

luminescence [19, 20].

It was previously found that synthesis using hydrothermal treatment in an autoclave produces LaF_3 nanoparticles with paramagnetic centers located predominantly within the particle bulk [21]. Hydrothermal treatment at 120°C yields a higher concentration of paramagnetic centers compared to the untreated sample, and with further increases in treatment temperature, the concentration of paramagnetic centers increases. The paramagnetic centers are most likely associated with OH groups, which replace F^- ions during hydrothermal treatment.

There are no published studies on nanoparticle synthesis using hydrothermal treatment in an autoclave at temperatures below 120°C. The study of the hydrothermal treatment temperature effect on particle size, crystallinity, and paramagnetic center concentration could be useful for obtaining nanoparticles with high crystallinity and minimal paramagnetic center concentration.

In this study, the effect of hydrothermal treatment temperature (60–140°C) in an autoclave on nanoparticle size, coherent scattering region size, and paramagnetic center concentration was studied for synthesized LaF_3 samples. Sensitivity of the ^{19}F nuclei magnetic relaxation to the presence of paramagnetic centers was observed. The optimal hydrothermal treatment temperature was determined for the synthesis of LaF_3 nanoparticles with the largest size and best crystallinity, while minimizing the paramagnetic centers content.

2. Experimental Methods

2.1. Materials

LaF_3 nanoparticles were synthesized by precipitation from colloidal solutions using a chloride reaction followed by hydrothermal treatment in an autoclave [21]. $LaCl_3{\cdot}7H_2O$ (99.99%), $KF{\cdot}2H_2O$ (99.9%), 69% HNO_3 (99.999%) from Sigma Aldrich (USA) and ultra-pure water from a Milli-Q deionization unit were used. 150 ml of KF solution with a concentration of 102.27 mM and 150 ml of $LaCl_3$ solution with a concentration of 17.04 mM were prepared. The acidity of the last solution was adjusted to pH = 2 using nitric acid. A solution of KF was added dropwise to a solution of $LaCl_3{\cdot}7H_2O$. Sample #1 was synthesized at room temperature without hydrothermal treatment in an autoclave. After thorough mixing for 30 minutes on a magnetic stirrer, the colloidal solution was subjected to hydrothermal treatment in a home-built stainless steel autoclave for 24 hours at temperatures of 60°C (sample #2), 90°C (sample #3), 100°C (sample #4), 110°C (sample #5), 120°C (sample #6), and 140°C (sample #7).

The resulting solution was purified from dissolved salts by centrifugation (Janetski K24; 12,000 rpm) and washing with deionized water. The final solution was dried on a flat surface in an air atmosphere at room temperature.

2.2. XRD method

The crystal phase of the synthesized LaF_3 samples was identified using a Bruker D8 Advance diffractometer with Cu Kα radiation (λ = 1.5418 Å) in Bragg–Brentano geometry. Powder diffraction patterns were recorded in the 2θ angle range of 20–60° with a scanning rate of 1.15° per minute.

2.3. TEM method

The morphology of the synthesized LaF_3 samples was characterized using a Hitachi HT7700 Exalens microscope (Japan) with an accelerating voltage of 100 kV. Samples for analysis were prepared by depositing a sample suspension onto a 3 mm thick copper grid covered with a continuous Formvar/carbon backing. The average particle size was estimated based on 1000 particles.

2.4. EPR measurements

Electron paramagnetic resonance (EPR) experiments were performed on a Bruker Elexsys E580 spectrometer in the X-band range (ν_{MW} = 9.6 GHz) at room temperature (T = 297 K). A $Cu^{2+}(DETC)_2$ sample dissolved in toluene with a spin concentration of 1.22 mM was used as

a reference. The concentrations of paramagnetic centers C_{pc} in the synthesized LaF_3 samples were estimated by double integration of the continuous-wave EPR spectra.

2.5. NMR measurements

NMR experiments were performed on a home-built pulsed NMR spectrometer [22] in a magnetic field of 3.65 T (frequency 145.5 MHz) at room temperature ($T = 297$ K). A Helmholtz coil (8 mm diameter) with two turns on each side, a 1 cm distance between turns, a 1.7 cm wire thickness, and inductive matching was used for the measurements. The spin–lattice relaxation time T_1 was measured using the saturation-recovery method with a 4.1 μs saturation pulse duration. The $\pi/2$ pulse duration was 3.5 μs. The spin–spin relaxation time T_2 was measured using a Hahn echo pulse sequence of 90° (3.5 μs) – 20 μs – 180° (3.5 μs) with phase cycling. The curves of the transverse magnetization decay and the longitudinal magnetization recovery of the fluorine nuclei were measured for all samples.

3. Results and Discussion

Figure 1 shows XRD powder patterns for all synthesized LaF_3 samples processed in an autoclave at different temperatures.

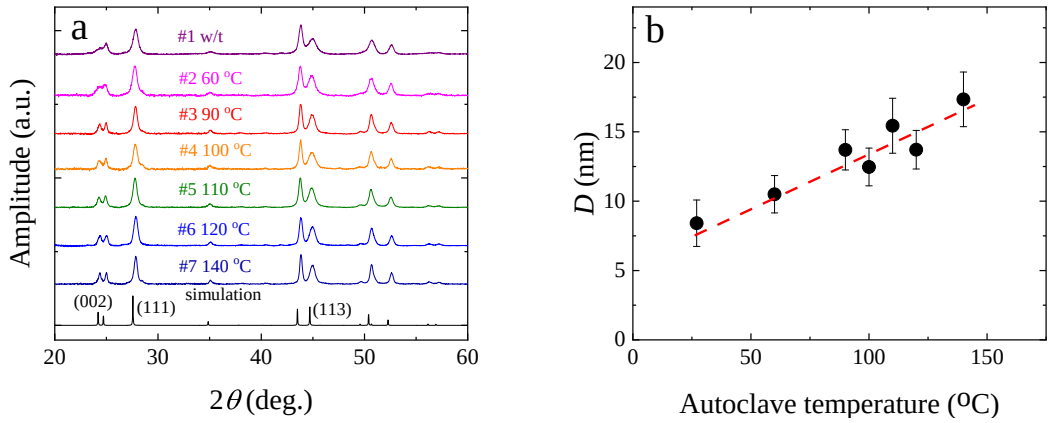

Figure 1. XRD powder patterns of LaF_3 samples #1–7 (a) and the dependence of the average size of the coherent scattering region on the hydrothermal treatment temperature (b).

As can be seen from Figure 1a, the XRD peaks of the synthesized samples are quite narrow, which indicates good crystallinity of the obtained samples. As the autoclave temperature increases, peaks in the planes, especially (002) and (110), are resolved.

The size of the coherent scattering region was estimated using the Scherrer equation [23]:

$$D = \frac{k\lambda}{\mathrm{FWHM} \cdot \cos(\theta)}, \tag{1}$$

where $k = 0.8$ is the form factor, λ is the wavelength of the X-ray radiation, θ is the peak position, and FWHM is the full width at half maximum of the peak.

The estimated sizes of the coherent scattering region for the synthesized LaF_3 samples are presented in Table 1.

The dependence of the estimated average size of the coherent scattering region on the temperature of the hydrothermal treatment is shown in Figure 1b. Along the planes (002), (111) and (113), as the temperature of the hydrothermal treatment in the autoclave increases, the average size of the coherent scattering region increases.

Images of LaF_3 synthesized particles obtained using TEM are shown in Figure 2a.

Histograms of particle size distribution were plotted from the TEM images data. The distribution histogram for sample #4 is shown in Figure 2b. The average sample sizes were determined

Table 1. The average size of the coherent scattering region D for LaF_3 samples #1–7.

Miller indices	Average size of coherent scattering region D, nm						
(hkl)	Sample #1	Sample #2	Sample #3	Sample #4	Sample #5	Sample #6	Sample #7
(002)	6.5	9.5	14.6	13.5	18.8	14.4	20.1
(111)	12.8	14.0	16.6	15.1	17.7	16.6	20.1
(113)	6.9	8.7	10.6	9.5	11.1	10.8	12.9

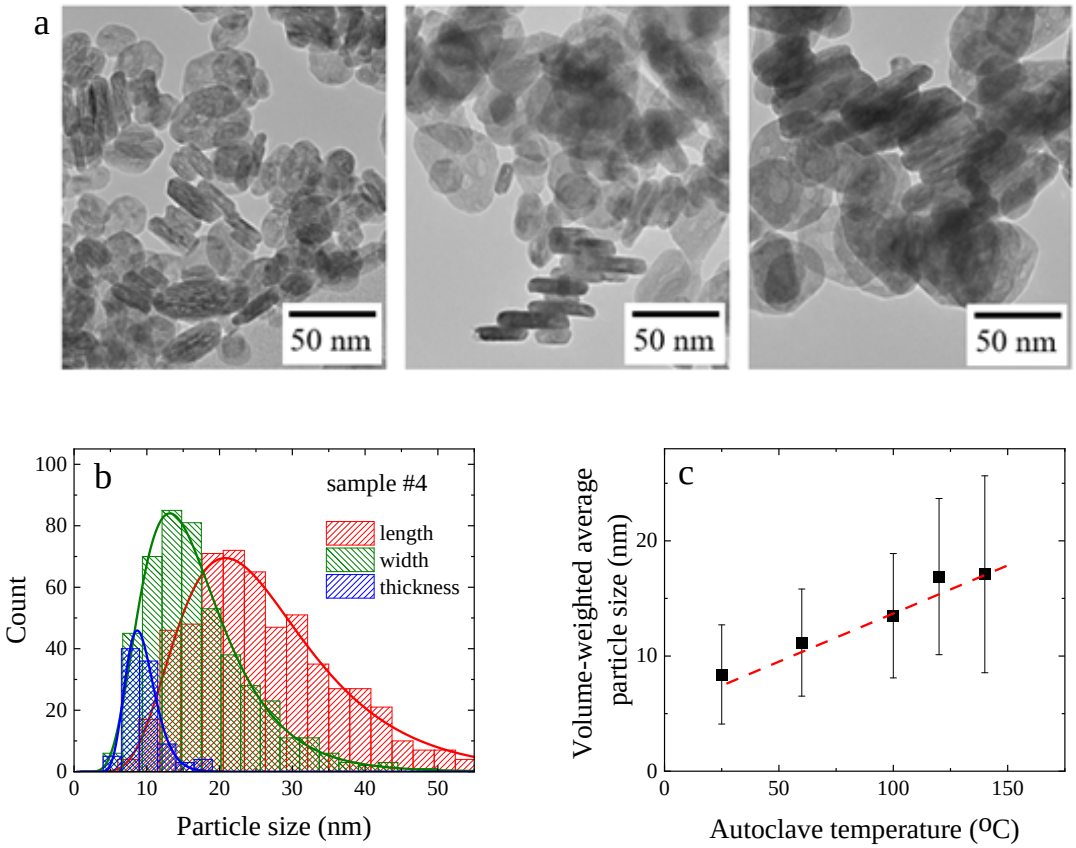

Figure 2. The TEM images of LaF_3 nanoparticles for samples with hydrothermal treatment in an autoclave at temperatures of 60°C (sample #2), 100°C (sample #4) and 140°C (sample #7) (a), histogram of particle size distribution for a sample at 100°C (sample #4) (b), volume-weighted average particle size dependence on the hydrothermal treatment temperature (c). The line is a visual guide.

by approximating the obtained histograms with a lognormal distribution. The characteristic size was taken at the maximum of the log-normal distribution, assuming these most abundant particles define the magnetic properties. The error was calculated as the root-mean-square deviation of the particle sizes relative to this maximum. Thus, the sizes of the synthesized LaF_3 samples were estimated using the TEM method data (length × width × height): $18 \times 13 \times 6$ nm, $21 \times 13 \times 9$ nm and $26 \times 16 \times 12$ nm (root-mean-square deviation is about 40% of the size value) for hydrothermal treatment temperatures of 60°C, 100°C and 140°C.

Figure 2c shows the volume-weighted average particle size dependence on the hydrothermal treatment temperature. It is observed that as the temperature of the hydrothermal treatment in the autoclave increases, the average particle size increases linearly. Thus, the average particle size increases with the coherent scattering region size. The difference between these values is less than 9%, which indicates high crystallinity of the samples.

The EPR spectrum of sample #4 measured at room temperature is shown in Figure 3a.

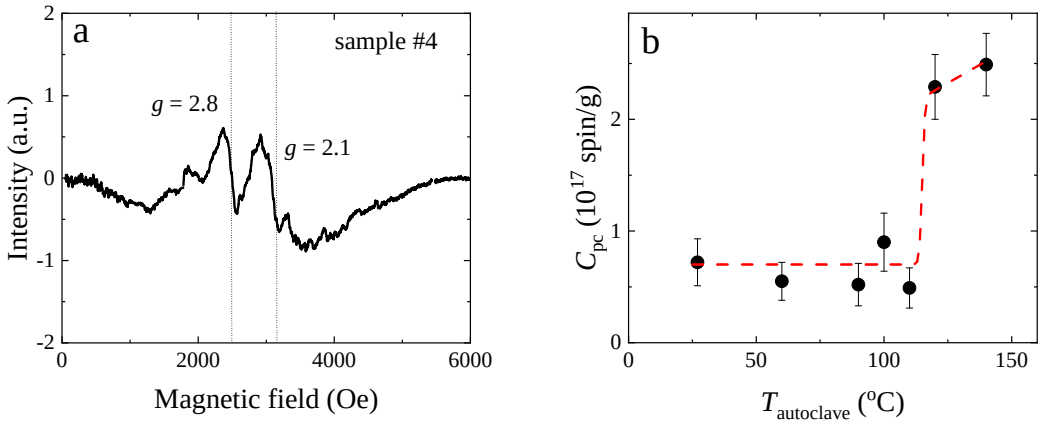

Figure 3. The EPR spectrum of the LaF_3 sample (sample #4) (a) and the dependence of the observed paramagnetic center concentration on the hydrothermal treatment temperature for all samples (b). The line is a visual guide.

As can be seen in Figure 3a, two lines can be distinguished – the first line with a g-factor of $g = 2.8$, which corresponds to the surface paramagnetic centers, and the second line with a g-factor of $g = 2.1$, corresponding to the OH groups located in the particle volume [21]. In this case, OH groups act as paramagnetic centers, the number of which increases during long-term hydrothermal treatment and are healed by fluorination. Paramagnetic centers are mainly located in the particle volume and are uniformly distributed.

After double integration of the continuous-wave EPR spectra, the estimated concentrations of paramagnetic centers in LaF_3 samples #1–7 are presented in Table 2, respectively.

Figure 3b shows the dependence of the observed paramagnetic center concentration on the hydrothermal treatment temperature. As can be seen from Figure 3b, the number of paramagnetic centers for samples with autoclave treatment below 120°C does not change with increasing temperature. When processed in an autoclave at a temperature of 120°C and above, the concentration of paramagnetic centers increases sharply. This behavior may be due to the fact that at temperatures above 120°C, the pressure of saturated water vapor is about 2 bar and then the pressure increases with increasing treatment temperature in the autoclave. Water under pressure demonstrates enhanced penetration into the particles, leading to a more intense incorporation of OH groups within the nanoparticle lattice.

The ^{19}F longitudinal magnetization recovery and transverse magnetization decay curves for sample #4 are shown in Figure 4.

As can be seen from Figure 4, the longitudinal magnetization recovery curve and the transverse magnetization decay curve are described by one-exponential equations:

$$M_z = B\left(1 - \exp\left(-\tau/T_1\right)\right), \tag{2}$$

$$M_{xy} = A\exp\left(-\tau/T_2\right). \tag{3}$$

Table 2 presents information about the synthesized samples: concentration of paramagnetic centers, and longitudinal and transverse relaxation times.

As shown in Table 2, the relaxation times T_1, T_2, and T_2^* exhibit a weak dependence on the concentration of paramagnetic centers. For the purpose of general estimation across all samples, these values can be averaged to approximately 1 s, 35 μs, and 8.5 μs, respectively. The accelerated longitudinal relaxation observed for sample #4 may be attributed to fluctuations

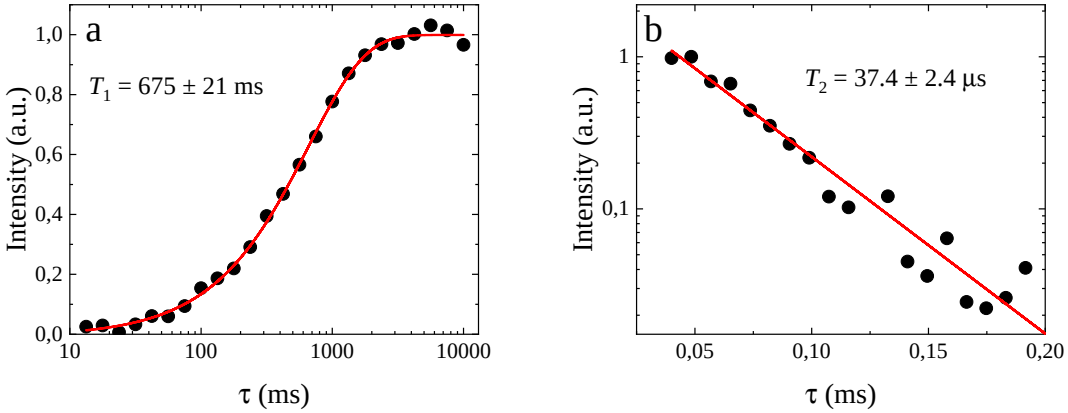

Figure 4. The longitudinal magnetization recovery (a) and transverse magnetization decay curves for sample #4 (b). Lines are fits by Eqs. 2–3.

Table 2. The estimated values of paramagnetic center concentrations, relaxation times T_1, T_2, and T_2^* for LaF_3 samples #1–7.

Sample #	Temperature in the autoclave, °C	C_{pc}, 10^{17} spin/g	T_1, ms	T_2, μs	T_2^*, μs
1	Without treatment	0.72 ± 0.21	974 ± 23	35.6 ± 0.9	7.39 ± 0.08
2	60	0.55 ± 0.17	1017 ± 58	40.3 ± 1.5	7.58 ± 0.04
3	90	0.52 ± 0.19	1036 ± 55	33.2 ± 1.1	9.03 ± 0.12
4	100	0.90 ± 0.26	675 ± 21	37.4 ± 2.4	6.92 ± 0.15
5	110	0.49 ± 0.18	1166 ± 62	39.7 ± 1.7	8.28 ± 0.07
6	120	2.29 ± 0.29	1063 ± 17	30.8 ± 3.1	9.61 ± 0.06
7	140	2.49 ± 0.28	1225 ± 42	32.4 ± 1.4	6.91 ± 0.11

occurring during the incorporation of OH groups into the crystal lattice at temperatures of 100°C.

In the presence of paramagnetic centers in the sample, electron-nuclear interactions usually play a dominant role in the rate of nuclear magnetic relaxation. A directly proportional dependence of T_1^{-1} of ^{19}F nuclei on the concentration of paramagnetic centers was observed in the BaF_2:Eu^{3+} compound [24]. Paramagnetic centers create fluctuating local magnetic fields on fluorine nuclei. Provided that the centers do not overlap and there is no exchange interaction between them, the contributions from each center are summed independently and T_1^{-1} linearly depends on the paramagnetic centers concentration [25].

When considering the transverse relaxation of nuclei, the main contribution to the line broadening is made by the predominance of the static dipole-dipole interaction ^{19}F – ^{19}F, which does not depend on the low concentration of introduced defects or impurities.

The rate of ^{19}F nuclear longitudinal local relaxation can be estimated using the following equation [26]:

$$T_{1\,\mathrm{local}}^{-1} = \frac{2}{5}(\mu_B g \gamma_I)^2 S(S+1)\frac{1}{r^6}\tau_c, \tag{4}$$

where μ_B is the Bohr magneton, g is the g-factor, γ_I is the gyromagnetic ratio of ^{19}F nuclei, $S = 1/2$ is the spin of paramagnetic centers, r is the distance between paramagnetic centers

and ^{19}F nuclei (the minimum value $r_{\min} = 0.3$ nm was estimated based on the distance between fluoride ions in the LaF_3 crystal lattice), and τ_c is the correlation time.

The electron relaxation time of paramagnetic centers can be estimated using the equation:

$$\tau_e^{-1} = \frac{g\mu_B}{\hbar}\Delta B, \tag{5}$$

where $\hbar$ is reduced Planck's constant, ΔB is the EPR line width, and the value $\tau_c \sim T_{2e}$ is about 10^{-10} s.

Thus, the local relaxation near the paramagnetic center is mainly determined by the relaxation time of the electron spins. The value of the local relaxation time of ^{19}F nuclei near paramagnetic centers is about 110 μs.

Magnetization transfer processes affect the average relaxation in the system through spin diffusion of fluorine nuclei and translational diffusion of fluorine ions.

Fluorines in LaF_3 nanoparticles typically move by hopping between lattice sites. Hopping of fluorine ions in the local magnetic field gradient leads to fluctuations in the nuclear field and additional relaxation, which operates predominantly near paramagnetic centers, where the magnetic field gradient is highest. Hopping of fluorine ions facilitates magnetization transfer from nuclei farther from the paramagnetic centers.

The characteristic time of translational diffusion movement of fluorine ions can be estimated as:

$$\tau_{\text{jump}} = \frac{a^2}{D}, \tag{6}$$

where $D \sim 10^{-13}$ cm^2/s is the coefficient of translational diffusion of fluorine ions [17, 27, 28], and $a \sim 3$ Å is the average jump distance. Therefore, the estimated value of τ_{jump} is about 10^{-2} s.

The characteristic time of nuclear spin diffusion:

$$\tau_{\text{spindiff}} = \frac{a^2}{D_s}, \tag{7}$$

where $D_s \sim 10^{-13}$ cm^2/s is the spin diffusion coefficient of fluorine nuclei [29], and $a \sim 3$ Å is the characteristic distance between the nuclei cores. The estimated value of $\tau_{\text{spin diff}}$ is about 10^{-2} s.

Thus, at room temperature, the characteristic time of translational diffusion is comparable to the characteristic time of nuclear spin diffusion.

As the radius of the diffusion barrier approaches half the distance between the paramagnetic centers, nuclear spin diffusion becomes hampered, which leads to a slowdown in the rate of nuclear magnetic relaxation. The radius of the diffusion barrier R_{diffbar} can be estimated using the equation:

$$R_{\text{diffbar}} = \sqrt[3]{\frac{g\mu_B}{\gamma_I \hbar N_I}}, \tag{8}$$

where N_I is the concentration of ^{19}F nuclei.

Half of the distance between the paramagnetic centers can be estimated using the equation:

$$R_{\text{pc}} = \frac{1}{2\sqrt[3]{C_{\text{pc}}}}. \tag{9}$$

For samples #1–5, the R_{pc} value is 7.1 nm, and the R_{diffbar} value is 2.3 nm. Thus, the concentrations of paramagnetic centers correspond to the fact that nuclear spin diffusion is not hampered.

The characteristic diffusion length of magnetization propagation due to hopping diffusion:

$$l = \sqrt{DT_1}. \tag{10}$$

The obtained estimated value of l is equal to 1 nm, which is of the same order as the radius of the diffusion barrier value R_{diffbar}. Therefore, it can be assumed that, despite the spin-diffusion barrier, hopping diffusion allows the magnetization to spread from nuclear spins near paramagnetic centers to distant spins.

Thus, the relaxation rate in LaF_3 nanoparticles appears to be determined by the spatial separation of two magnetization transfer mechanisms. In the immediate vicinity of the paramagnetic center, where the ^{19}F–^{19}F dipole-dipole interaction is highly inhomogeneous and spin diffusion is presumably suppressed due to the spread of Larmor frequencies, translational diffusion of fluoride ions could play a dominant role. It is likely in this region, where the local field is most inhomogeneous, that F^- jumps effectively alter the precession phase of nuclear spins, ensuring relaxation. Far from the paramagnetic centers, where field gradients are small, polarization transfer is expected to be mediated by conventional nuclear spin diffusion. The two mechanisms most likely do not compete but rather complement each other on different spatial scales, resulting in efficient averaged relaxation.

The maximal average longitudinal relaxation rate of the system can be estimated as:

$$T_1^{-1} = \langle T_{1\,\text{local}}^{-1} \rangle_V = \frac{4\pi}{V} \int_a^{R_{\text{pc}}} \frac{2}{5} (\mu_B g \gamma_I)^2 S(S+1) \frac{1}{r^6} \tau_c r^2 \, dr = \frac{2}{5} (\mu_B g \gamma_I)^2 S(S+1) \frac{1}{a^3} \frac{1}{R_{\text{pc}}^3} \tau_c. \tag{11}$$

For simplicity, the Fermi contact interaction of fluorine nuclei and paramagnetic centers, the approximate value of the diffusion coefficient, the approximate value of the action region boundaries of nuclear spin diffusion and translational diffusion of fluorine ions were not taken into account. The estimated longitudinal relaxation time in the system is 1.5 s, while the experimental longitudinal relaxation time is approximately 1 s. Thus, the calculated and experimental values are of the same order of magnitude. Differences between experimental and theoretical values can most likely be attributed to earlier simplifying assumptions.

Data on the magnetic relaxation of fluoride nuclei and the concentration of paramagnetic centers confirm that the magnetic properties of nanoscale LaF_3 do not change significantly up to 110°C.

4. Conclusion

A series of LaF_3 nanoparticles was synthesized using hydrothermal treatment in an autoclave at temperatures 60–140°C. As the hydrothermal treatment temperature in the autoclave increased, the size of the synthesized particles increased, as well as the estimated size of the coherent scattering region. However, the concentration of paramagnetic centers, which is most likely associated with the substitution of fluoride ions with OH groups, remained relatively constant (within experimental error) up to 110°C. For a sample with hydrothermal treatment in an autoclave at a temperature of 120°C, a sharp increase in the concentration of paramagnetic centers occurs. This may be due to an increase in saturated water vapor pressure. The magnetic relaxation of ^{19}F nuclei in LaF_3 nanoparticles was considered.

Thus, it is important to take into account that during hydrothermal treatment of a colloidal solution of LaF_3 nanoparticles in an autoclave, paramagnetic centers associated with OH groups appear, which non-linearly depend on the hydrothermal temperature in an autoclave. A sample of LaF_3 nanoparticles with subsequent autoclave treatment at 110°C is optimal for practical use since it has high crystallinity with a minimum content of paramagnetic centers.

The work may be useful in studying the effect of synthesis on structure and magnetic properties in a wide class of materials.

Data availability statement

The data supporting the main findings of this study are available from the corresponding authors upon reasonable request.

Acknowledgments

This work was financially supported by the Russian Science Foundation (Project No. 23-72-10039).

References

1. Hong J.Q., Zhang L.H., Zhang P.X., Wang Y.Q., Hang Y., *Journal of Alloys and Compounds* **646**, 706 (2015).
2. Tressaud A., Wang Z., Tang Y., Li Q., *Responsive Materials* **3**, e70031 (2025).
3. Rocha U., Kumar K.U., Jacinto C., Villa I., Sanz-Rodríguez F., del Carmen Iglesias de la Cruz M., Juarranz A., Carrasco E., van Veggel F.C.J.M., Bovero E., Solé J.G., Jaque D., *Small* **10**, 1141 (2014).
4. Diamente P.R., van Veggel F.C.J.M., *Journal of Fluorescence* **15**, 543 (2005).
5. Kasturi S., Marikumar R., Vaidyanathan S., *Luminescence* **33**, 897 (2018).
6. Talik E., Zajdel P., Guzik A., Skrzypek D., Lipińska L., Michalska M., *Journal of Alloys and Compounds* **616**, 556 (2014).
7. Couwenberg I., Görller-Walrand C., *Journal of Alloys and Compounds* **275**, 388 (1998).
8. Gazizulina A.M., Alakshin E.M., Baibekov E.I., Gazizulin R.R., Zakharov M.Yu., Klochkov A.V., Korableva S.L., Tagirov M.S., *JETP Letters* **99**, 149 (2014).
9. Rakhmatullin R.M., Pudovkin M.S., Semashko V.V., *Magnetic Resonance in Solids* **21**, 12 (2019).
10. Shakurov G.S., Semashko V.V., Morozov O.A., *Magnetic Resonance in Solids* **27**, 25301 (2025).
11. Pudovkin M.S., Zelenikhin P.V., Shtyreva V.V., Evtugyn V.G., Salnikov V.V., Nizamutdinov A.S., Semashko V.V., *Journal of Nanoparticle Research* **21**, 184 (2019).
12. Wang K., Ma J., He M., Gao G., Xu H., Sang J., Wang Y., Zhao B., Cui D., *Theranostics* **3**, 258 (2013).
13. Nafziger R.H., Lincoln R.L., Riazance N., *Journal of Inorganic and Nuclear Chemistry* **35**, 421 (1973).
14. Bosch S., Leinfellner N., Quesnel E., Duparre A., Ferre-Borrull J., Guenster S., Ristau D., *Optical and Infrared Thin Films* **4094**, 15, SPIE (2000).
15. Jacobsohn L.G., Kucera C.J., James T.L., Sprinkle K.B., DiMaio J.R., Kokuoz B., Yazgan-Kukouz B., DeVol T.A., Ballato J., *Materials* **3**, 2053 (2010).
16. Rahman P., Green M., *Nanoscale* **1**, 214 (2009).
17. Sinitsyn V.V., Lips O., Privalov A.F., Fujara F., Murin I.V., *Journal of Physics and Chemistry of Solids* **64**, 1201 (2003).
18. Hehlen M.P., Boncher W.L., Melgaard S.D., Blair M.W., Jackson R.A., Littleford T.E., Love S.P., *In Laser Refrigeration of Solids VII* **9000**, 14, SPIE (2014).
19. Przybylińska H., Zhydachevskyy Y., Grochot A., Wołoś A., Stasiv V., Glowacki M., Kaminska A., Ubizskii S., Berkowski M., Suchocki A., *The Journal of Physical Chemistry C* **126**, 743 (2021).
20. Ishida H., Tobita S., Hasegawa Y., Katoh R., Nozaki K., *Coordination Chemistry Reviews* **254**, 2449 (2010).

21. Garaeva A.M., Murzakhanov F.F., Boltenkova E.I., Mukhamadullin B.M., Klimovitskii A.E., Mamin G.V., Alakshin E.M., *The Journal of Physical Chemistry C* **129**, 3076 (2025).
22. Kuzmin V.V., Bogaychuk A.V., Nekrasov I.K., Safiullin K.R., Salakhov M.H., Alakshin E.M., Klochkov A.V., Tagirov M.S., *Magnetic Resonance in Solids* **21**, 19401 (2019).
23. Scherrer P., *Nachrichten von der Gesellschaft der Wissenschaften, Göttingen. Mathematisch-Physikalische Klasse* **26**, 98 (1918).
24. Miller J.R., Mahendroo P.P., *Physical Review* **174**, 369 (1968).
25. Rorschach Jr. H.E., *Physica* **30**, 38 (1964).
26. Abragam A., *Principles of Nuclear Magnetism*, Oxford University Press (1961).
27. Aalders A.F., Arts A.F.M., de Wijn H.W., *Physical Review B* **32**, 5412 (1985).
28. Sher A., Solomon R., Lee K., Muller M.W., *Physical Review* **144**, 593 (1966).
29. Shen L., *Physical Review* **172**, 259 (1968).